Coincidence spectroscopy of high-lying Rydberg states produced in strong laser fields

Seyedreza Larimian,[1] Sonia Erattupuzha,[1] Christoph Lemell,[2] Shuhei Yoshida,[2] Stefan Nagele,[2] Raffael Maurer,[1] Andrius Baltuška,[1] Joachim Burgdörfer,[2] Markus Kitzler,[1] and Xinhua Xie (谢新华)[1,3,*]

[1]*Photonics Institute, Vienna University of Technology, A-1040 Vienna, Austria, European Union*

[2]*Institute for Theoretical Physics, Vienna University of Technology, A-1040 Vienna, Austria, European Union*

[3]*Institute of Theoretical Chemistry, University of Vienna, A-1090 Vienna, Austria, European Union*

(Received 13 April 2016; published 1 September 2016)

We demonstrate the detection of high-lying Rydberg states produced in strong laser fields with coincidence spectroscopy. Electron emission *after* the interaction of strong laser pulses with atoms and molecules is measured together with the parent ions in coincidence measurements. These electrons originate from high-lying Rydberg states with quantum numbers from $n \sim 20$ up to $n \lesssim 120$ formed by frustrated field ionization. Ionization rates are retrieved from the measured ionization signal of these Rydberg states. Simulations show that both tunneling ionization by a weak dc field and photoionization by blackbody radiation contribute to delayed electron emission on the nano- to microsecond scale. Furthermore, the dependence of the Rydberg-state production on the ellipticity of the driving laser field indicates that such high-lying Rydberg states are populated through electron recapture. The present experiment provides detailed quantitative information on Rydberg production in strong-field interaction.

DOI: 10.1103/PhysRevA.94.033401

I. INTRODUCTION

Ionization of atoms and molecules by strong laser fields is the starting point for a multitude of interesting phenomena, e.g., high harmonic generation or molecular fragmentation [1]. For sufficiently strong laser fields corresponding to intensities of the order of $I \sim 10^{14}$ W/cm^2, atoms and molecules are ionized via tunneling ionization, i.e., an electron passes through the potential barrier of the combined Coulomb and laser fields. After tunneling, electrons are steered by the laser field and most of them will eventually escape the Coulomb field of the remaining ion core. However, a fraction of them are recaptured into highly excited states by the ionic Coulomb field. This process, frequently referred to as frustrated field ionization, leads to the formation of high-lying Rydberg states with binding energies extending from a fraction of an eV to values of μeV near threshold [2–9].

Very high-lying Rydberg states with principal quantum numbers $n \approx 100$ are quantum objects of mesoscopic size allowing for studies of the border between the quantum and the classical worlds [10]. Formation and destruction of such mesoscopic objects can be described by semiclassical and classical methods [11]. Recent experiments on high harmonic generation and electron wave-packet interferometry indicate the important contribution of such excited states to different processes [12–16] including ionization and molecular dissociation processes [17–21].

To explore the production process and the properties of high-lying Rydberg states formed in the strong-field interaction with atoms and molecules, direct observation of such states is required. Traditionally, zero kinetic energy photoelectron spectroscopy is applied to study weakly bound states in atoms and molecules [22]. In the case of strong-field interaction, however, the ionization signal from Rydberg states is completely overshadowed by the dominant laser-field–induced ionization signal from the target and the residual gas in the interaction chamber. Therefore, the signal from Rydberg states cannot be extracted easily. Signatures of postpulse ionization of high-lying Rydberg states have been found recently in the "zero-energy structures" of photoelectrons [17,18]. However, the information one can obtain on the Rydberg states involved from the momentum distribution of photoelectrons is rather limited because of the overlap with the ionization signal induced by strong laser fields.

In this article, we report on coincidence measurements of electrons and ions separated from each other by the ionization process using a cold target recoil ion momentum spectrometer (COLTRIMS) [23,24]. The delayed signal of weak-dc-field–induced ionization of high-lying Rydberg states with principal quantum numbers from $n \sim 20$ up to $n \lesssim 120$ populated during strong-field interaction of atoms and molecules can be well distinguished from the prompt strong-field ionization signal and retains a very high signal-to-noise ratio. Supported by simulations, we identify two contributions with characteristic time constants governing the delayed ionization of Rydberg states: (i) a strongly dc-field–dependent and (ii) a nearly dc-field-independent contribution attributed to emission from long-lived Stark resonances and photoionization by blackbody radiation (BBR) at room temperature [25]. We also determine the dependence of the strong-field–induced Rydberg population on the ellipticity of the exciting laser pulse [6].

II. EXPERIMENT

Measurements were carried out with laser pulses from a home-built Ti:sapphire laser amplifier with a center wavelength of 795 nm, a repetition rate of 5 kHz, and a pulse duration (full width at half maximum of the intensity) of 25 fs. The peak laser intensity is of the order of $I \sim 10^{14}$ W/cm^2 with a peak electric-field strength of $F_0 \sim 2.7 \times 10^8$ V/cm. The laser beam is crossed with an atomic or molecular gas jet in a conventional COLTRIMS apparatus [23,24]. In the target region, a weak homogeneous dc field from $F_{dc} = 0.1$ V/cm up to $F_{dc} = 30$ V/cm is applied to accelerate charged particles to the detectors. An additional homogeneous magnetic field of

*xinhua.xie@tuwien.ac.at

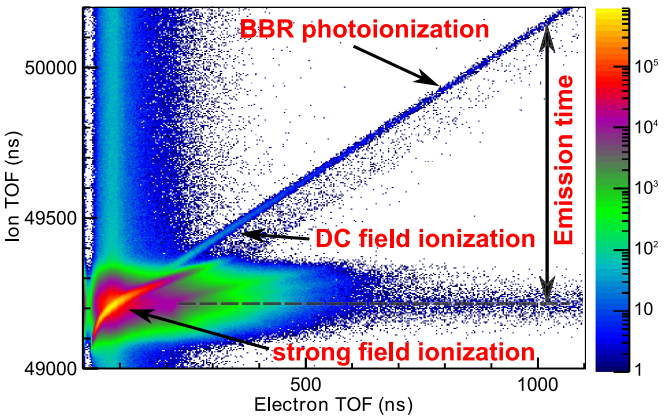

FIG. 1. PEPICO spectrum for argon atoms interacting with 25 fs laser pulses with peak electric-field strength of $F_0 = 3.9 \times 10^8$ V/cm (intensity $I = 2 \times 10^{14}$ W/cm^2) and a dc-field strength of $F_{\rm dc} = 1.5$ V/cm. Electron emission during and after the laser pulse can be distinguished in this spectrum.

12.3 gauss ensures 4π detection of fast electrons. More details of the experimental setup can be found in, e.g., [12,26].

In contrast to the usual data evaluation procedure applied in COLTRIMS experiments (retrieval of three-dimensional electron and ion momenta) for electrons and ions separated *during* the laser pulse, we analyze only the arrival times of particles with momenta $p_{e,i} \approx 0$ a.u. with the aim to study postpulse ionization of target atoms and molecules excited by the laser pulses. A typical photoelectron-photoion-coincidence (PEPICO) spectrum for argon atoms interacting with a 25 fs laser pulse ($I = 2 \times 10^{14}$ W/cm^2, $F_{\rm dc} = 1.5$ V/cm) features a main peak at electron time of flight (TOF) of 85 ns and ion TOF of 49205 ns (Fig. 1) representing photoemission in the strong field of the laser pulse and setting the reference for the delayed emission. Postpulse ionization events, i.e., an electron and its parent ion being separated after the conclusion of the exciting laser pulse with initial momenta $p_{e,i} \approx 0$ a.u., are registered along the diagonal with unit slope from which the ionization times of the excited argon atoms can be inferred directly. Clear signals for postpulse ionization were found for emission times extending up to 80 microseconds after conclusion of the laser pulse. Our interpretation of the PEPICO spectrum is confirmed by classical-trajectory simulations to determine the flight times of ions with initial momenta $p_i = 0$ a.u. assuming strong field or postpulse ionization by the weak dc field reproducing the parabolic main feature (Fig. 1) and the straight line on the diagonal, respectively. A clear separation of the two features becomes possible only after about 200 ns, as shown in Fig. 1.

III. RESULTS AND DISCUSSION

Measurements were performed for three atomic gases (argon, helium, and neon) and six molecular targets (hydrogen, methane, ethylene, acetylene, 1,3-butadiene, and hexane). We interpret the long-time coincidences as postpulse ionization of high-lying Rydberg states generated by frustrated field ionization which could be observed for all three atomic gases and for hydrogen, methane, ethylene, and acetylene molecular targets, but not for 1,3-butadiene and hexane. This is most likely related to the instability of high-lying Rydberg states of such large molecules leading to molecular dissociation on time scales shorter than the delayed detection of Rydberg states starting after a few hundred nanoseconds [27,28]. In the following, we quantitatively analyze coincidence spectra of postpulse ionized Rydberg states of argon in detail. We find for these Rydberg states delayed emission times extending to about hundred microseconds. Similar results were found for all other target species for which this process was observed.

A. Weak dc-field ionization and BBR-induced photoionization

When ions recapture electrons released during the laser pulse, high-n states of the atom with $n \gtrsim n_\alpha = \sqrt{\alpha}$ are populated [17,29], with $\alpha = F_0/\omega^2$ the quiver amplitude (atomic units are used throughout unless otherwise noted). For the laser parameters of Fig. 1, $\sqrt{\alpha} \approx 4.5$ and the dominant angular momenta of these states have been found to be close to $L \approx \sqrt{2F_0}/\omega = 6$ [29]. These estimates are corroborated by semiclassical simulations for argon atoms (for details of the simulation, see, e.g., [17]). Figure 2 shows the final-energy distribution of electrons for the subensemble with $E < 0$ a.u., i.e., for electrons remaining bound to the ion core after conclusion of the pulse. Near the energy corresponding to a hydrogenic level with $n = 5$ [the shaded area indicates the semiclassical energy interval ($n_{\rm cl} = 5 \pm 1/2$) assigned to the quantum number n], we find a steep rise of the distribution of final energies and a weak decrease of "occupation" for very high n states. The corresponding simulated angular momentum distribution of recaptured electrons is peaked at $L = 6$ with a sharp cutoff at $L = 7$ (not shown).

In the presence of the weak dc field $F_{\rm dc}$, Rydberg states very close to the continuum threshold and well above the potential barrier can be ionized. Due to "fast" laser excitation compared to the "slow" dynamics of Rydberg electrons, the lowest n_F Rydberg state being ionized can be estimated using the diabatic field ionization threshold $F_{\rm dc} = 1/(9n_F^4)$. For $F_{\rm dc} = 3$ V/cm, Rydberg Stark states with $n > n_F \simeq 120$ are accessible to postpulse over-the-barrier ionization. Such states have a

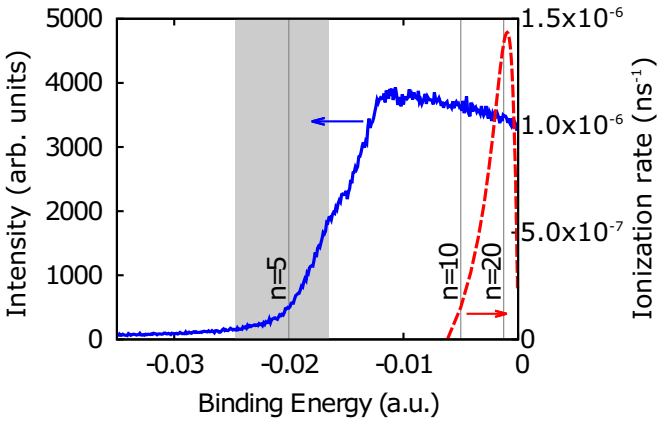

FIG. 2. Simulated distribution of total electron energies after conclusion of the laser pulse for the parameters of Fig. 1 (blue solid line, left axis). The rate for blackbody radiation (red dashed line, right axis) at a temperature of $T = 300$ K ($\hbar\omega_{\rm BBR} \approx 0.0026$ eV) contributes to the total BBR ionization for $n \gtrsim 10$ with a maximum near $n = 23$.

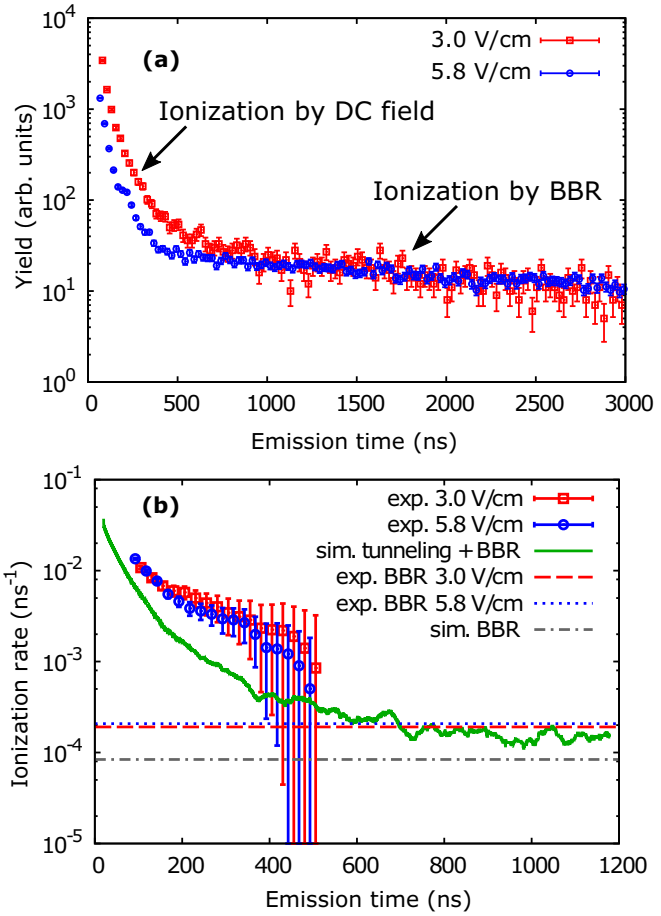

FIG. 3. (a) Intensity $I(\tau)$ of the signal of postpulse ionized Rydberg states of argon (diagonal in Fig. 1) as a function of the emission time τ for two field strengths $F_{\rm dc}$ with the same laser interaction condition (peak intensity of 1.5×10^{14} W/cm^2). (b) Ionization rate of Rydberg states derived from the data in (a) in comparison with simulated tunneling ionization rates for $F_{\rm dc} = 3$ V/cm and blackbody radiation (BBR) rates.

diameter of more than 0.5 μm ($\langle r \rangle_n \propto n^2$) and typical orbital periods $\tau_{\rm orb} = 2\pi n^3$ of more than hundred picoseconds.

The emission time from strong-field–induced Rydberg population can be derived from the intensity distribution along the diagonal in Fig. 1 [plotted in Fig. 3(a)]. The postpulse ionized yield $I(\tau)$ strongly depends on the field strength $F_{\rm dc}$ of the external dc field [Fig. 3(a)]. The smaller yield for $F_{\rm dc} = 5.8$ V/m is directly related to the faster depletion of Rydberg states susceptible to the external field leaving a smaller number of excited atoms $\gtrsim$200 ns after the laser pulse, i.e., the time we can clearly separate laser-ionized from postpulse coincidences. In contrast, the corresponding ionization rates $\Gamma = -d\ln[I(\tau)]/d\tau$ [Fig. 3(b)] derived from the data in Fig. 3(a) appear to be rather insensitive to the value of $F_{\rm dc}$. The rate decreases from about $\Gamma \approx 0.01$ ns^{-1} at $\tau = 100$ ns to about $\Gamma \approx 0.001$ ns^{-1} at $\tau = 500$ ns. For emission times longer than 650 ns, the ionization rate becomes nearly constant with a value of $\Gamma \approx 2 \times 10^{-4}$ ns^{-1}. The constant ionization rates for the two field strengths, indicated by blue dotted (at 2.08×10^{-4} ns^{-1}) and red dashed (at 1.91×10^{-4} ns^{-1}) horizontal lines in Fig. 3(b), are

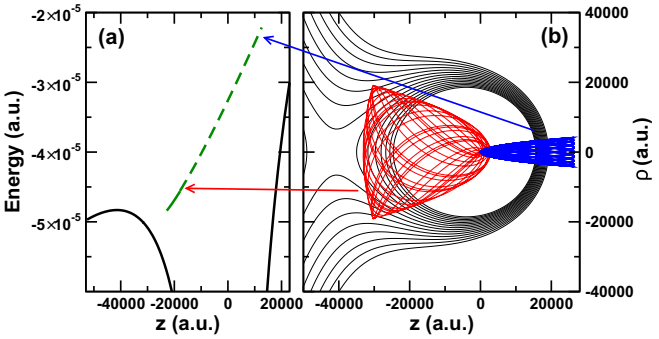

FIG. 4. (a) Potential energy (black solid line) along the z axis and eigenenergies (dashed green line) of hydrogenic Stark states with $n = 121, m = 0$ in a weak dc field of $F_{\rm dc} = 3$ V/cm. The energy is plotted as a function of the expectation value $\langle z \rangle$ of the associated Stark state. The solid part of the line indicates states with tunneling rate $>10^{-7}$ ns^{-1}, and the dashed part indicates states with a smaller rate. (b) Typical classical trajectories of red- and blueshifted Stark states with corresponding energies indicated by arrows. Contour lines of the potential landscape are shown as thin black lines.

derived from the measured signals in Fig. 3(a) for emission times larger than 650 ns fitted by exponential functions. For comparison, the strong-field tunneling ionization rate for the argon ground state ($E_{\rm bind} = -15.76$ eV) for a field strength of $F_0 = 3.4 \times 10^8$ V/cm (intensity $I = 1.5 \times 10^{14}$ W/cm^2) is, according to the Ammosov-Delone-Krainov formula [30], about 2×10^5 ns^{-1}, i.e., many orders of magnitude larger.

In order to identify processes underlying the delayed emission on the nano- to microsecond scale, different ionization channels must be considered: over-the-barrier ionization, tunneling ionization, and blackbody radiation induced photoionization and photoexcitation to above-barrier states. For a field strength $F_{\rm dc} = 3$ V/cm, which we focus on in the following, the saddle of the potential landscape lies energetically near $n = 102$ of the unperturbed hydrogenic spectrum. In the dc field, the critical principal quantum number is shifted to $n_F = 121$ (Fig. 4). For states lying well below the Stark barrier, tunneling rates are negligibly small on the nano- to microsecond time scale that the experiment is sensitive to. We have performed long-time classical trajectory simulations for the dc-field ionization process. Starting conditions were determined by the phase-space distribution of the corresponding subensemble of the semiclassical laser-atom simulation at the conclusion of the laser pulse. The electrons follow stretched elliptic trajectories with the ionic core in one focal point. For states close to n_F, the classical trajectories are bound [Fig. 4(b)]. In particular, the blueshifted state of the $n = 121$ manifold points in the direction opposite to the saddle and features lifetimes that are long compared to the ionization times accessible in the experiment. Even most of the redshifted states localized on the downhill side miss the saddle because of a relatively large transverse energy $p_\perp^2/2$. Quantum mechanically, the latter have tunneling rates $>10^{-7}$ ns^{-1} (corresponding to quantum numbers $n = 121$, parabolic quantum number $n_1 < 10$, and $m = 0$), indicated with a solid line in the energy diagram in Fig. 4(a), while states with larger n_1 have ionization rates $<10^{-7}$ ns^{-1} [dashed part of the line in Fig. 4(a)]. The applicability of hydrogenic Stark ionization rates to the present data for strong-field

ionization of argon follows from the fact that frustrated field ionization forms predominantly non-core-penetrating high-ℓ states which are well approximated by hydrogenic states. Scattering at the nonhydrogenic core of argon could transfer initially blueshifted Stark states to states oriented towards the saddle, leading to non-negligible contributions of tunneling ionization [31,32]. However, in the presence of the dc field, the core scattering rate is strongly suppressed and too small to efficiently depopulate the long-lived Stark resonances during the experimentally accessible time interval. We find that only a very small subset of the populated Rydberg states contributes to the experimental signal: states with $n \geqslant 123$ are field ionized on a time scale well below 100 ns, the starting point of our resolved coincidence measurements; for states with $n < n_F$, the tunneling rates are by far too small.

On the (sub)microsecond time scale, ionization by BBR present in the experiment performed at room temperature, $\langle \hbar\omega_{\rm BBR}\rangle \approx 0.026$ eV, becomes non-negligible. BBR may either directly ionize the atom or excite it to even higher Rydberg states, eventually leading to over-the-barrier or tunneling ionization [31,32]. In Fig. 2, the BBR rate is shown together with the distribution of electron energies at the conclusion of the pulse, indicating that states with $n \gtrsim 10$ can be directly photoionized.

The time-dependent Rydberg population of $m = 0$ states with parabolic quantum number n_1, $\rho(n,n_1,t)$, is governed by the rate equation

$$\dot{\rho}(n,n_1,t) = -[T(n,n_1) + R_{\rm BBR}(n)]\rho(n,n_1,t)\,, \qquad (1)$$

with $T(n,n_1)$ the tunneling ionization rate and $R_{\rm BBR}(n)$ the blackbody radiation photoionization rate. We determine the effective time-dependent ionization rate,

$$\Gamma_{\rm eff}(t) = -\frac{d\ln\left[\sum_{n,n_1}\rho(n,n_1,t)\right]}{dt}, \qquad (2)$$

by Monte Carlo sampling of decay channels starting with an energy-independent spectral excitation density $\rho(n,0)dn/dE \approx c_0$ formed by frustrated field ionization (Fig. 2, [17]). The resulting ionization rates for Rydberg states with n in the range of 121 to 136 are independent of n (within the statistical error). Therefore, the calculated rates are rather insensitive to the n distribution of Rydberg states after laser excitation [Fig. 3(b)]. The initial rapid decay of the ionization rate within 500 ns can be attributed to tunneling of redshifted Stark states.

The blackbody radiative ionization rate $R_{\rm BBR}(n)$, while overall small, increases with decreasing n down to quantum numbers $n_{\rm BBR}$ where the binding energy matches $\langle\omega_{\rm BBR}\rangle$ [31–33]. In the present case, $n_{\rm BBR} \approx 20$. Summing over the range $n < n_F$, the BBR ionization rate is estimated as $R_{\rm BBR}(n) = 8.4\times10^{-5}$ ns^{-1}. Additionally, the BBR-induced excitation rate is about 1×10^{-5} ns^{-1}. These contributions are comparable to the ionization rate from tunneling. Total ionization rates $\sim 2\times10^{-4}$ ns^{-1} including tunneling and BBR-induced ionization yield good agreement with the observed time dependence of the delayed emission for times approaching one microsecond. Residual differences can be attributed to the effect of stray fields and inhomogeneities of the field.

The simulation suggests that the present time-delayed PEPICO spectra provide direct access to long-lived Stark resonances in very high Rydberg states and to the population of the Rydberg manifolds extending from $n_{\rm BBR} \approx 10$ to $n_F \approx 120$ formed by frustrated field ionization.

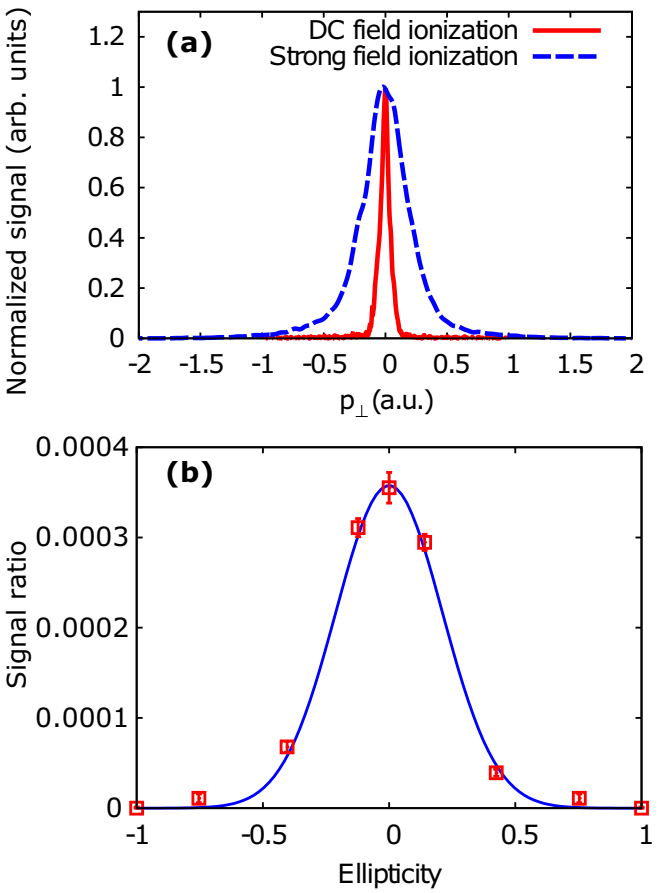

FIG. 5. (a) Projected momentum distribution of delayed electron emission perpendicular to the direction of $F_{\rm dc}$ (the red solid line) and of prompt electrons perpendicular to the laser polarization direction (the blue dashed lines). (b) Measured ratio between time-integrated signal of delayed ionization of high-lying Rydberg states of Ar and the strong laser field ionized Ar as a function of laser ellipticity (red points). The blue solid line is a guide to the eye.

B. Momentum distribution and dependence on laser polarization

With our reaction microscope, we also measure the initial momenta of the released Rydberg electrons. As expected for a "zero-energy structure," the average momentum of the postpulse ionized electrons is very small. Moreover, we find the momentum distribution perpendicular to the direction of the dc field ($\Delta p_\perp^{\rm dc} = 0.04$ a.u.) to be much narrower than the transverse distribution of the prompt electron emission by strong-field ionization $\Delta p_\perp = 0.4$ a.u. [Fig. 5(a)],

$$T(n,p_\perp) = C\exp\left(-\frac{2}{3n^3F}\right)\exp\left(-\frac{p_\perp^2}{nF}\right). \qquad (3)$$

For strong-field emission, the width of the momentum distribution has been previously derived [34] to give $\Delta p_\perp = \sqrt{2\log 2\cdot F/|E_{\rm bind}|} = 0.41$ a.u., in close agreement with our data [Fig. 5(a)]. Applying the same expression to high Rydberg

states $n \approx 100$ yields $\Delta p_{\perp}^{\mathrm{dc}} \approx 0.004$ a.u., which is much narrower than the experimental momentum resolution of about 0.04 a.u. Likewise, BBR ionized electrons are expected to have a momentum distribution peaked near zero momentum, $|p| \ll \sqrt{2\langle\omega_{\mathrm{BBR}}\rangle} \approx 0.04$. Therefore, the width of the delayed peak in Fig. 5(a) is primarily given by our experimental resolution.

We tested the dependence of the strength of the signal on the polarization ellipticity ε of the exciting laser pulse, which is known to have a strong influence on the probability for recapturing electrons after tunneling and, hence, on $\rho(n,0)$. To this end, we used a laser with an intensity of $I = 2.5 \times 10^{14}$ W/cm^2 at a dc-field strength of $F_{\mathrm{dc}} = 3$ V/cm [Fig. 5(b)]. As expected, the Rydberg signal has a maximum for linearly polarized laser fields and drops to 0 when increasing the ellipticity up to $\varepsilon = 1$ (circular polarization) [6]. This ellipticity dependence is similar to that of high harmonic generation from strong laser interaction [35–37] and to the ellipticity dependence of the occupation of Rydberg states with $n < 30$ in helium [8,38]. Such dependence is consistent with the fact that the formation of high-lying Rydberg states is a rescattering process with the released electron ending up close to the ionic core with small momentum at the conclusion of the pulse. In laser pulses with ellipticity $\varepsilon \neq 0$, the electron is driven away from the core, effectively suppressing the recapture process.

IV. CONCLUSIONS

We have presented the coincidence detection of high-lying Rydberg states populated during the interaction of intense laser pulses with atoms and molecules. Recapture of tunnel ionized electrons, frequently referred to as frustrated field ionization, appears to be a very general process as we have observed its signatures for various atomic and molecular target species. The electron-ion coincidence spectroscopy allows one to identify two major contributions: tunneling ionization of Rydberg Stark resonances lying just above the saddle point of the potential landscape in the presence of a weak dc field, and photoionization by blackbody radiation of lower-lying Rydberg states. A gradual transition from the tunneling dominated regime was observed for the field strength $F_{\mathrm{dc}} = 3$ V/cm near $\tau \approx 500$ ns. Tuning the strength of the external dc-field strength F_{dc} may open the pathway to selectively probe Stark resonances close to the principal quantum number $n_F \lesssim 3^{-1/2} F_{\mathrm{dc}}^{-1/4}$ near the saddle threshold for over-the-barrier ionization as only a very small number of n shells (in the present case, 2) have tunneling rates of the proper order of magnitude such that they are accessible with the present PEPICO setup. The experimental data are consistent with a nearly constant spectral excitation density of the Rydberg manifold above $n \gtrsim 20$. We also find that frustrated field ionization is strongly dependent on the ellipticity of the driving laser pulse.

With the multiparticle coincidence detection capability of a COLTRIMS, the electron-ion coincidence spectroscopy can be directly applied to reveal the importance of high-lying Rydberg states in laser-induced multiple ionization and to channel-resolved studies of molecular dissociation processes involving high-lying Rydberg states.

ACKNOWLEDGMENTS

We would like to thank Armin Scrinzi and Chii-Dong Lin for fruitful discussions. This work was supported by the Austrian Science Fund (FWF): Grants No. P25615-N27, No. P21141-N16, No. P28475-N27, No. P21463-N22, and No. P27491-N27, Special Research Programs No. SFB-041 ViCoM and No. SFB-049 NextLite, and doctoral program Solids4Fun No. W1243. Calculations were performed in part on the Vienna Scientific Cluster (VSC).

[1] T. Brabec and F. Krausz, Rev. Mod. Phys. **72**, 545 (2000).
[2] F. Benvenuto, G. Casati, and D. L. Shepelyansky, Phys. Rev. A **45**, R7670(R) (1992).
[3] M. P. de Boer and H. G. Muller, Phys. Rev. Lett. **68**, 2747 (1992).
[4] R. Grobe and M. V. Fedorov, J. Phys. B **26**, 1181 (1993).
[5] R. R. Jones, D. W. Schumacher, and P. H. Bucksbaum, Phys. Rev. A **47**, R49(R) (1993).
[6] R. R. Jones, D. You, and P. H. Bucksbaum, Phys. Rev. Lett. **70**, 1236 (1993).
[7] S. Yoshida, C. O. Reinhold, J. Burgdörfer, W. Zhao, J. J. Mestayer, J. C. Lancaster, and F. B. Dunning, Phys. Rev. A **73**, 033411 (2006).
[8] T. Nubbemeyer, K. Gorling, A. Saenz, U. Eichmann, and W. Sandner, Phys. Rev. Lett. **101**, 233001 (2008).
[9] U. Eichmann, A. Saenz, S. Eilzer, T. Nubbemeyer, and W. Sandner, Phys. Rev. Lett. **110**, 203002 (2013).
[10] F. B. Dunning, J. J. Mestayer, C. O. Reinhold, S. Yoshida, and J. Burgdörfer, J. Phys. B **42**, 022001 (2009).
[11] T. F. Gallagher, *Rydberg Atoms* (Cambridge University Press, Cambridge, 2005), Vol. 3.
[12] X. Xie, S. Roither, D. Kartashov, E. Persson, D. G. Arbó, L. Zhang, S. Gräfe, M. S. Schöffler, J. Burgdörfer, A. Baltuška, and M. Kitzler, Phys. Rev. Lett. **108**, 193004 (2012).
[13] M. Chini, X. Wang, Y. Cheng, H. Wang, Y. Wu, E. Cunningham, P.-C. Li, J. Heslar, D. A. Telnov, S.-I. Chu *et al.*, Nat. Photon. **8**, 437 (2014).
[14] X. Xie, Phys. Rev. Lett. **114**, 173003 (2015).
[15] Y. Deng and X. Xie, Phys. Rev. A **91**, 043414 (2015).
[16] D. G. Arbó, S. Nagele, X.-M. Tong, X. Xie, M. Kitzler, and J. Burgdörfer, Phys. Rev. A **89**, 043414 (2014).
[17] B. Wolter, C. Lemell, M. Baudisch, M. G. Pullen, X.-M. Tong, M. Hemmer, A. Senftleben, C. D. Schröter, J. Ullrich, R. Moshammer, J. Biegert, and J. Burgdörfer, Phys. Rev. A **90**, 063424 (2014).
[18] H. Liu, Y. Liu, L. Fu, G. Xin, D. Ye, J. Liu, X. T. He, Y. Yang, X. Liu, Y. Deng, C. Wu, and Q. Gong, Phys. Rev. Lett. **109**, 093001 (2012).
[19] Q. Li, X.-M. Tong, T. Morishita, C. Jin, H. Wei, and C. D. Lin, J. Phys. B **47**, 204019 (2014).
[20] R. Minns, D. Lazenby, F. Hall, N. Jones, R. Patel, and H. Fielding, Mol. Phys. **112**, 1808 (2014).

[21] H. Lv, W. Zuo, L. Zhao, H. Xu, M. Jin, D. Ding, S. Hu, and J. Chen, Phys. Rev. A **93**, 033415 (2016).
[22] K. Muller-Dethlefs and E. W. Schlag, Annu. Rev. Phys. Chem. **42**, 109 (1991).
[23] J. Ullrich, R. Moshammer, A. Dorn, R. Doerner, L. P. H. Schmidt, and H. Schmidt-Boecking, Rep. Prog. Phys. **66**, 1463 (2003).
[24] R. Dörner, V. Mergel, O. Jagutzki, J. U. L. Spielberger, R. Moshammer, and H. Schmidt-Böcking, Phys. Rep. **330**, 95 (2000).
[25] T. F. Gallagher and W. E. Cooke, Phys. Rev. Lett. **42**, 835 (1979).
[26] X. Xie, K. Doblhoff-Dier, S. Roither, M. S. Schöffler, D. Kartashov, H. Xu, T. Rathje, G. G. Paulus, A. Baltuška, S. Gräfe, and M. Kitzler, Phys. Rev. Lett. **109**, 243001 (2012).
[27] X. Zhou, P. Ranitovic, C. W. Hogle, J. H. D. Eland, H. C. Kapteyn, and M. M. Murnane, Nat. Phys. **8**, 232 (2012).
[28] A. S. Bogomolov, B. Grüner, S. A. Kochubei, M. Mudrich, and A. V. Baklanov, J. Chem. Phys. **140**, 124311 (2014).
[29] D. G. Arbó, C. Lemell, S. Nagele, N. Camus, L. Fechner, A. Krupp, T. Pfeifer, S. D. López, R. Moshammer, and J. Burgdörfer, Phys. Rev. A **92**, 023402 (2015).
[30] M.-V. Ammosov, N.-B. Delone, and V.-P. Krainov, Sov. Phys. JETP **64**, 1191 (1986).
[31] W. P. Spencer, A. G. Vaidyanathan, D. Kleppner, and T. W. Ducas, Phys. Rev. A **26**, 1490 (1982).
[32] I. I. Beterov, D. B. Tretyakov, I. I. Ryabtsev, A. Ekers, and N. N. Bezuglov, Phys. Rev. A **75**, 052720 (2007).
[33] I. L. Glukhov, E. A. Nekipelov, and V. D. Ovsiannikov, J. Phys. B **43**, 125002 (2010).
[34] L. Arissian, C. Smeenk, F. Turner, C. Trallero, A. V. Sokolov, D. M. Villeneuve, A. Staudte, and P. B. Corkum, Phys. Rev. Lett. **105**, 133002 (2010).
[35] Y. Liang, S. Augst, M. V. Ammosov, S. Lazarescu, and S. L. Chin, J. Phys. B **28**, 2757 (1995).
[36] A. Flettner, J. König, M. Mason, T. Pfeifer, U. Weichmann, R. Düren, and G. Gerber, Eur. Phys. J. D **21**, 115 (2002).
[37] M. Möller, Y. Cheng, S. D. Khan, B. Zhao, K. Zhao, M. Chini, G. G. Paulus, and Z. Chang, Phys. Rev. A **86**, 011401 (2012).
[38] A. S. Landsman, A. N. Pfeiffer, C. Hofmann, M. Smolarski, C. Cirelli, and U. Keller, New J. Phys. **15**, 013001 (2013).